September 2006

A Comparison of LSM, LSF, and LSCo for Solid Oxide Electrolyzer Anodes

Wensheng Wang
University of Pennsylvania

Yingyi Huang
University of Pennsylvania

Sukwon Jung
University of Pennsylvania

John M. Vohs
University of Pennsylvania, vohs@seas.upenn.edu

Raymond J. Gorte
University of Pennsylvania, gorte@seas.upenn.edu

A Comparison of LSM, LSF, and LSCo for Solid Oxide Electrolyzer Anodes

Abstract

Composite electrodes of yttria-stabilized zirconia (YSZ) with $La_{0.8}Sr_{0.2}MnO_3$ (LSM), $La_{0.8}Sr_{0.2}FeO_3$ (LSF), and $La_{0.8}Sr_{0.2}CoO_3$ (LSCo) were prepared and tested as solid oxide electrolyzer (SOE) anodes and solid oxide fuel cell (SOFC) cathodes at 973 K, using cells with a YSZ electrolyte and a Co-ceria-YSZ counter electrode. The LSM-YSZ electrode was activated by cathodic polarization but the enhanced performance was found to be unstable during electrolysis, with the electrode impedance increasing to near its unenhanced state after 24 h. LSF-YSZ and LSCo-YSZ electrodes exhibited a nearly constant impedance, independent of current density, during both SOE and SOFC operation. The performance of an LSF-YSZ composite for electrolysis current densities above 200 mA/cm^2 was unaffected by changing the O_2 partial pressure from ~10^{-2} to 1 atm, while the lower O_2 pressure harmed the performance of the LSCo-YSZ composite. The implications of these results for the characterization and optimization of SOE anodes is discussed.

A Comparison of LSM, LSF, and LSCo for Solid Oxide Electrolyzer Anodes

Wensheng Wang, Yingyi Huang, Sukwon Jung, John M. Vohs, and Raymond J. Gorte
Department of Chemical and Biomolecular Engineering
University of Pennsylvania
Philadelphia, PA 19104

Abstract

Composite electrodes of yttria-stabilized zirconia (YSZ) with $La_{0.8}Sr_{0.2}MnO_3$ (LSM), $La_{0.8}Sr_{0.2}FeO_3$ (LSF), and $La_{0.8}Sr_{0.2}CoO_3$ (LSCo) were prepared and tested as solid oxide electrolyzer (SOE) anodes and solid oxide fuel cell (SOFC) cathodes at 973 K, using cells with a YSZ electrolyte and a Co-ceria-YSZ counter electrode. The LSM-YSZ electrode was activated by cathodic polarization but the enhanced performance was found to be unstable during electrolysis, with the electrode impedance increasing to near its un-enhanced state after 24 h. LSF-YSZ and LSCo-YSZ electrodes exhibited a nearly constant impedance, independent of current density, during both SOE and SOFC operation. The performance of an LSF-YSZ composite for electrolysis current densities above 200 mA/cm^2 was unaffected by changing the O_2 partial pressure from ~10^{-2} atm to 1 atm, while the lower O_2 pressure harmed the performance of the LSCo-YSZ composite. The implications of these results for the characterization and optimization of SOE anodes is discussed.

1. Introduction

Solid oxide electrolyzers (SOE) hold promise for the efficient production of H_2 from electricity because electrolysis at elevated temperatures is advantageous for both thermodynamic and kinetic reasons [1]. As in all electrolyzers, the basic operating principle involves reduction at the cathode of water ($H_2O + 2e^- \rightarrow H_2 + O^{2-}$) from a H_2-H_2O mixture and rejection at the anode of O_2 ($O^{2-} \rightarrow \frac{1}{2}O_2 + 2e^-$) to the air. Because of the similarity with solid oxide fuel cells (SOFC), most prototype SOE have used the same materials as those used for SOFC: yttria-stabilized zirconia (YSZ) as the electrolyte, a Ni-YSZ ceramic-metallic (cermet) composite at the H_2-H_2O electrode, and an electrode based on Sr-doped $LaMnO_3$ (LSM) at the air electrode [2,3].

An ideal SOE would electrolyze water at the Nernst potential, but the applied potential in a real SOE must be higher so as to overcome the ohmic losses in the electrolyte and the over-potential losses in the electrodes. While there have been extensive investigations into electrode losses in SOFC, relatively few studies have been published on SOE. Despite the fact that many studies of SOFC have shown excellent performance at temperatures below 1073 K, a recent report on SOE states the operating temperature of current SOE are limited to near 1273 K "because of insufficient performance of the state-of-the-art electrolyte and electrodes at low temperatures" [4]. There are also apparent discrepancies in the published literature. For example, one paper claims that the over-potentials at a given current density are very different under SOE and SOFC conditions with Ni-YSZ|YSZ|LSM-YSZ cells [5], while another report with the same set of materials claims the area-specific resistance is identical over a relatively large range of current densities in both fuel-cell and electrolyzer regimes [3].

Because the air electrode is often the limiting component for SOFC operating on H_2, we set out to investigate the effect of composition on the air electrodes for SOE. It is well known that SOFC cathodes based on Sr-doped $LaCoO_3$ (LSCo) and Sr-doped $LaFeO_3$ (LSF) exhibit much lower polarization losses than cathodes based on LSM [6-8]. A primary reason for using LSM-based cathodes is that LSM-YSZ electrodes are easier to fabricate. Unlike LSF and LSCo, LSM can be sintered together with YSZ at relatively high temperatures without forming insulating layers of $La_2Zr_2O_7$ and $SrZrO_3$ [9]. However, in our laboratory, we have demonstrated that we can prepare electrodes based on LSF and LSCo without forming insulating phases by adding the perovskites to a porous YSZ matrix that has previously been sintered to high temperatures [10-12]. LSCo-YSZ cathodes prepared by impregnation exhibit an excellent initial

performance, but slowly deactivate due to solid-state reactions that occur even at this low temperature [11]. Based on initial results, SOFC cathodes composed of LSF-YSZ composites appear to be reasonably stable, at least at temperatures below 1073 K.

We were also interested in investigating the effect of polarization history on LSM-YSZ electrodes. Many groups have observed a reversible decrease in the impedance of LSM-YSZ SOFC cathodes upon electrode polarization [12-23]. While the mechanism for this decrease has not been definitively established, there seems to be universal agreement that the activation process involves partial reduction of the LSM. Because anodic polarization results in an oxidizing environment, any reversible enhancement resulting from reduction of LSM should be lost during electrolysis. Indeed, a very recent study has reported that the impedance of activated LSM-YSZ electrodes increases with time during anodic polarization [24].

In this study, we will demonstrate that there is a good correlation between performance of air electrodes in SOFC and SOE. As reported previously [24], we found that LSM-YSZ electrodes show poor performance under electrolysis conditions because the enhancement that occurs upon cathodic polarization is lost during electrolysis. By contrast, LSF-YSZ electrodes exhibit excellent and stable performance.

2. Experimental

Almost all of the electrodes in this work were prepared by impregnation methods that have been described in previous papers [10-12]. The first step in preparing these electrodes involved casting several YSZ tapes, with and without pore formers, and then laminating these tapes together. Firing the laminated tapes to 1823 K resulted in a YSZ wafer a dense electrolyte layer having a porous layer on one or both sides. The LSF-YSZ ($La_{0.8}Sr_{0.2}FeO_3$) [10], LSCo-YSZ ($La_{0.8}Sr_{0.2}CoO_3$) [11], and LSM-YSZ ($La_{0.8}Sr_{0.2}MnO_3$) [12] composites were prepared by impregnation with the appropriate nitrate salts into 50-μm thick porous layer to a loading of 40-wt% perovskite. The H_2-H_2O electrodes were 300-μm thick with 15-wt% CeO_2 and 30-wt% Co, prepared by impregnation of aqueous solutions of $Co(NO_3)_2$ and $Ce(NO_3)_3$. A more complete description of these electrodes and their characteristics are given in previous publications [10-12]. In some experiments, LSM-YSZ electrodes were prepared by pasting a mixture of 50-wt% LSM ($La_{0.8}Sr_{0.2}MnO_3$, Praxair technologies) and YSZ powders onto a dense YSZ wafer and calcining the mixture to 1523 K. In agreement with our previous work [12,21], results for LSM-

YSZ electrodes prepared by impregnation of LSM into porous YSZ were essentially indistinguishable from "pasted" electrodes.

All of the experiments in this study were performed on 1.25-cm diameter button cells that had an active area of 0.35 cm^2 for the air electrodes. The electronic contacts were made using Ag wire and Ag paste on the air electrodes and Au wire with Au paste on the Co-ceria-YSZ electrodes. Each cell was sealed onto a 1.0-cm alumina tube using a ceramic adhesive (Aremco, Ultra-Temp 516). The mole fraction of water inside the alumina tube was maintained at 15% by bubbling 150 ml/min of H_2 through distilled water held at a controlled temperature. To avoid condensation, all tubing was maintained at 373 K using heating tapes. The alumina tube with the cell was placed inside a second tube whose O_2 partial pressure could be controlled by flowing in 300 ml/min of air, O_2, or N_2.

Impedance data were recorded in the galvanostatic mode using a Gamry Instruments potentiostat, with a frequency range from 0.01 Hz to 100 kHz and perturbation amplitude of 5 mV. Impedance data were acquired under different dc polarizations, negative currents for fuel-cell mode and positive currents for electrolysis. To obtain V-i curves, dc potential sweeps were performed in the potentiostat mode over a potential range from 0 to 1.5 V. Because only a single wire was attached to each electrode, there was an additional 0.2 $\Omega \cdot cm^2$ ohmic component in all of the results reported here due to the lead wires.

3. Results

V-i curves for potentials between 0.5 V and 1.5 V and impedance data under electrolysis at 140 mA/cm^2 for three cells with LSM-YSZ, LSF-YSZ, and LSCo-YSZ electrodes, operating at 973 K, are shown in Fig. 1. In each case, the Co-ceria-YSZ electrodes were exposed to flowing mixtures containing 15% H_2O and H_2, and pure O_2 was supplied to the air-side electrode. Initially, the cells were shorted for 10 min to cathodically polarize the air-side electrodes; the data in Fig. 1a) were then acquired while increasing the potential from 0 V to 1.5 V at 20 mV/s. The impedance data were obtained immediately after reaching 1.5 V. Fig. 1a) shows that the open-circuit voltage (OCV) for each of the cells was close to the Nernst potential, 1.07 V, based on the gas compositions at the electrodes. Also, the relationships between potential and current densities were reasonably linear for each of the three cells, implying that the electrode impedances do not undergo dramatic changes in going from fuel-cell to electrolysis

mode of operation. The slope of the V-i curve was lowest for the cell with the LSCo-YSZ electrode and highest for the cell with the LSM-YSZ electrode.

The impedance data in Fig. 1b) help to explain the causes for potential losses in each of the cells. First, the ohmic losses, associated primarily with the 100-μm thick electrolytes, were similar for all three cells, 0.65 $\Omega \cdot cm^2$ for the LSM-YSZ and LSF-YSZ cells and 0.55 $\Omega \cdot cm^2$ for the LSCo-YSZ cell. Second, the total impedances of the LSF-YSZ, 1.0 $\Omega \cdot cm^2$, and LSCo-YSZ, 0.7 $\Omega \cdot cm^2$, cells were equal to slopes of the V-i curves measured at OCV, while the total impedance of the LSM-YSZ cell, 1.3 $\Omega \cdot cm^2$, was slightly larger than the slope. As will be discussed shortly, the results for the LSM-YSZ cell were affected by the polarization history and the total impedance of this cell was changing with time while the measurements were being made. For the LSCo-YSZ cell, the total electrode polarization loss, determined from the span under the arc in the Cole-Cole plot, was less than 0.2 $\Omega \cdot cm^2$. Since both electrodes contribute to this loss, 0.2 $\Omega \cdot cm^2$ is an upper bound on the impedance of the Co-ceria-YSZ electrode at 973 K. For the LSF-YSZ cell, the total electrode polarization loss was 0.3 $\Omega \cdot cm^2$.

The effect of polarization history on LSM-YSZ composite was investigated more carefully using a cell with a "pasted" LSM-YSZ electrode, with the results shown in Figs. 2 through 4. The data in Fig. 2 used 15% H_2O in H_2 at the Co-ceria-YSZ electrode and air, 21% O_2, at the anode. The cell was heated to 973 K at OCV, after which the current density was measured as the cell potential was ramped to 1.5 V at 20 mV/s. Next, this cell was operated in the fuel-cell mode at a current density of 570 mA/cm^2 for 1 h and the electrolysis V-i curve measured again. The results show that there was a significant drop in the cell overpotential, the difference between the measured potential and OCV, at all current densities following cathodic polarization of the electrode. Finally, the cell was allowed to operate in the electrolysis mode at 285 mA/cm^2 for 24 h, after which the V-i curve was measured again. While the performance of the cell did not completely revert back to its initial state, the cell performance after 24 h of electrolysis operation was similar to its performance prior to cathodic polarization of the LSM-YSZ electrode.

The OCV impedance data in Fig. 3 were obtained during a second fuel-cell/electrolysis polarization cycle on the same cell. In these measurements, the cell was operated in the fuel-cell mode at a current density of 570 mA/cm^2 for 1 h, followed by operation in the electrolyzer mode at a current density of 285 mA/cm^2. At various times, the impedance spectra were taken rapidly

(~2 min) at OCV before returning the cell to the electrolysis mode. The impedance data confirm that the changes in the cell are associated with the impedance of the electrodes. The initial, total electrode impedance of the cell was nearly 4.0 $\Omega \cdot cm^2$, based on the difference between the total cell impedance, 4.5 $\Omega \cdot cm^2$, and the ohmic resistance, 0.7 $\Omega \cdot cm^2$. After polarization, the total cell impedance decreased to 1.8 $\Omega \cdot cm^2$, a value that is higher than that shown in Fig. 1b) primarily because the cathodic polarization current was much lower in this experiment but partially because air, rather than O_2, was fed to the anode. The total cell impedance increased steadily with time under electrolysis conditions. It is also noteworthy that the increased electrode impedance is associated with a characteristic frequency of approximately 1 Hz, a value typical of diffusion processes. In a previous paper from our laboratory, results indicated that LSM spreads over YSZ surfaces under oxidizing conditions and that the limiting process on LSM-YSZ electrodes prior to polarization is the diffusion of oxygen anions through the LSM film [12,25].

The changes that occurred in the LSM-YSZ cell over time are shown in another way in Fig. 4. Here, the potential that was required to maintain an electrolysis current of 285 mA/cm^2 is plotted as a function of time after fuel-cell polarization. That the increasing potential was related to changes in the electrode impedance is demonstrated by the good correspondence between increasing cell potential and the total electrode impedances, taken from Fig. 3.

Unlike LSM-YSZ electrodes, electrodes based on LSF are not affected by polarization and are stable under electrolysis conditions, as shown in Fig. 5. Here, the cell potential is again plotted as a function of time for a current density of 285 mA/cm^2 in the electrolysis mode, using air at the anode and 15% H_2O in H_2 at the cathode and operating at 973 K. The data in Fig. 5 also demonstrate that the Co-ceria-YSZ cathode must be stable, so that the results in Figs. 2 through 4 can only be explained by changes in the LSM-YSZ electrode.

The effects of current density on electrode impedance for the LSF-YSZ and LSCo-YSZ cells are shown in Fig. 6. These measurements were performed using pure O_2 at the perovskite electrode and 15% H_2O in H_2 at the Co-ceria-YSZ electrode. With LSF-YSZ, there is very little change in the total electrode impedance in going from 30 mA/cm^2 in the fuel-cell mode to 140 mA/cm^2 in the electrolysis mode, in agreement with the data in Fig. 1a) that showed an almost linear V-i relationship. Increasing the electrolysis current density to 430 mA/cm^2 caused both the ohmic resistance and the electrode impedance to decrease slightly. The results for LSCo-YSZ, Fig. 6b), also showed a slightly decreased electrode impedance at higher electrolysis currents.

Finally, we examined the effect of O_2 partial pressures on the LSF-YSZ and LSCo-YSZ electrodes in Fig. 7, again using 15% H_2O in H_2 at the cathode and a temperature of 973 K. Because we were interested in observing the effect of large changes in $P(O_2)$, the data in these figures was taken while flowing either pure O_2 or pure N_2 into the electrolysis anode compartment. Since the O_2 concentration decreases exponentially with time when it is removed by displacement with N_2 in a mixed vessel and since O_2 is formed by electrolysis, some O_2 was always present at the anode, even under flowing N_2. Based on the measured OCV of 0.8 V and the ratio of O_2 production rates to that of the N_2 flow rate, we estimate that the $P(O_2)$ varied between 10^{-4} to 10^{-2} atm for electrolysis in flowing N_2.

Fig. 7a) shows that, for the cell with the LSF-YSZ electrode at electrolysis current densities over 200 mA/cm^2, the V-i relationship is unaffected by the $P(O_2)$ in the anode compartment. This is probably not surprising because anodic polarization at the three-phase boundary (TPB) will cause the perovskite to experience a $P(O_2)$ many times that of the true $P(O_2)$. For the cell with the LSCo-YSZ electrode, the cell performance with O_2 flowing in the anode compartment is actually better than the performance with flowing N_2. The reason for this is unclear, although it is possible that the effect is associated with the ease with which LSCo is reduced.

4. Discussion

There are several important conclusions that can be drawn from the results of this study. First, it is clear that there is a direct correspondence between the performance of LSM, LSF, and LSCo as SOE anodes and their performance as SOFC cathodes. These electrodes do not exhibit a dramatic change in their impedance in going from anodic to cathodic polarization. Indeed, we did not even observe a discontinuity at OCV. While the linear relationship between cell potential and current density, extending from SOFC to SOE operation, could be due to compensation between the fuel-side and air-side electrodes for a single set of materials, the fact that linearity is observed for three different air-side electrodes matched to the same fuel-side electrode demonstrates that the electrode impedance cannot vary significantly for any of the electrode materials.

The deactivation that occurred for the LSM-YSZ electrode operating under anodic polarization suggests that this material is not going to be as effective for SOE anodes as it is for SOFC cathodes. As pointed out in the Introduction, it is necessary to cathodically polarize LSM-

YSZ cathodes for them to exhibit good performance at lower temperatures. The activation associated with cathodic polarization has been associated with partial reduction of the LSM and this state cannot be maintained under anodic polarization.

Electrodes based on LSF and LSCo do not require polarization in order for them to exhibit a low impedance as SOFC cathodes and they maintain this low impedance as SOE anodes. There is the issue of long-term stability with these materials, given their tendency to undergo solid-state reactions with YSZ. LSCo films on YSZ have been shown to undergo reaction, even at 973 K [26], and a study of LSCo-YSZ cathodes from our laboratory showed a steady decrease in performance over a period of 100 h [11]. However, LSF-YSZ composites appear to be reasonably stable as SOFC cathodes, at least for operation below 1073 K [10]. There is the obvious question of whether anodic polarization might affect the long-term stability of these composites, either by stabilizing or destabilizing them; but the short-term stability at 973 K is evident from our study, at least for LSF-YSZ.

The results from changing the O_2 partial pressure at the anode reveal a potential difficulty in the measurement of electrode performance. Often, performance is determined by measuring an overpotential, the difference between the actual cell potential and the Nernst potential at a given current density. In addition to the fact that overpotential measurements for a specific electrode require the use of a reference electrode, which can provide erroneous results unless the cell geometry is properly chosen [27], there is the additional problem of defining the Nernst potential at the three-phase boundary. If the results in Fig. 7a) had been plotted in terms of electrode overpotentials, they would show that the anode overpotential is greatly reduced for operation in O_2 compared to operation in N_2. A similar problem occurs in the measurement of SOFC anode overpotentials, for which it has been reported that water catalyzes the oxidation of H_2. In that case, too, it has been shown that the apparent reduction in overpotential upon the addition of water is an artifact [28].

It is interesting to consider our results in terms of Butler-Volmer kinetics. The Butler-Volmer model views the overpotential as a "temperature" required to overcome reaction barriers, so that one should observe a logarithmic dependence between cell potential and current density near OCV. However, it seems clear that there is no evidence for non-linear behavior in the V-i curves, implying that any activation barriers to be overcome by the overpotential must be small.

Furthermore, any Butler-Volmer parameters calculated from plots of overpotential versus logarithm of the current density should be viewed with suspicion.

Finally, the results presented here demonstrate the great promise of solid oxide electrolyzers. A reasonable electrolysis current density of 285 mA/cm^2 was achieved at a modest temperature of 973 K and a potential of only 1.2 V. Because almost two thirds of the cell impedance in that cell was associated with the lead wires and the 100-μm YSZ electrolyte, much higher current densities could have been achieved by simply using a thinner electrolyte, even without additional optimization of the cells. Furthermore, this performance was achieved with a low H_2O:H_2 ratio at the cathode and no observable penalty for having concentrated O_2 at the anode. Obviously, further work is required to fully understand and develop the potential of SOE.

Acknowledgements

This work was funded by the U.S. Department of Energy's Hydrogen Fuel Initiative (grant DE-FG02-05ER15721).

5. Conclusions

The performance of LSM-YSZ, LSF-YSZ, and LSCo-YSZ composites as SOE anodes corresponds closely to their performance as SOFC cathodes at 973 K. LSF-YSZ and LSCo-YSZ composites exhibit impedances that are essentially independent of current and the same under anodic and cathodic polarization. Because LSM-YSZ composites show good performance only after cathodic activation and because this activated state is lost during operation as an SOE, LSM-based electrodes do not appear to be optimal. Finally, there was no evidence for an exponential dependence between cell potential and current density, implying that it is not appropriate to use the Butler-Volmer Equation to analyze electrode performance.

6. References

1. W. Doenitz, R. Schmidberger, E. Steinheil, and R. Streicher, *Int. J. Hydrogen Energy*, **5**, 55 (1980).
2. W. Donitz and E. Erdle, *Int. J. Hydrogen Energy*, **10**, 291 (1985).
3. J. E. O'Brien, C. M. Stoots, J. S. Herring, P. A. Lessing, J. J. Hartvigsen, and S. Elangovan, *Trans. ASME*, **2**, 156 (2005).
4. H. Uchida, N. Osada, M. Watanabe, *Electrochem. Sol.-State Lett.*, **7**, A500 (2004).
5. K. Eguchi, T. Hatagishi, and H. Arai, *Solid State Ionics*, **86**, 1245 (1996).

6. S. P. Simner, J. R. Bonnett, N. L. Canfield, K. D. Meinhardt, J. P. Shelton, V. L. Sprenkle, and J. W. Stevenson, *Journal of Power Sources*, **113**, 1 (2003).
7. Chiba, R., F. Yoshimura, and Y. Sakurai, *Solid State Ionics*, **152-153**, 575 (2002).
8. S. P. Simner, J. R. Bonnett, N. L. Canfield, K. D. Meinhardt, V. L. Sprenkle, and J. W. Stevenson,, *Electrochemical and Solid-State Letters*, 5, A173 (2002).
9. K. Kleveland, M. A. Einarsrud, C. R. Schmidt, S. Shamsili, S. Faaland, K. Wiik, T. Grande, *J. Am. Ceram. Soc.*, **82**, 729 (1999).
10. Y. Huang, J. M. Vohs, and R. J. Gorte, *Journal of The Electrochemical Society*, **151**, A646 (2004).
11. Y. Huang, J. M. Vohs, and R. J. Gorte, Journal of The Electrochemical Society, **151**, A1592 (2004).
12. Y. Huang, J. M. Vohs, and R. J. Gorte, *Journal of The Electrochemical Society*, **152**, A1347 (2005).
13. S. P. Jiang, J. G. Love, *Solid State Ionics*, **138**, 183-190 (2001).
14. M. J. Jorgensen, S. Primdahl, M. Mogensen, *Electrochim. Acta* , **44**, 4195-4201(1999).
15. F. H. van Heuveln, H. J. M. Bouwmeester, *Journal of the Electrochemical Society*, **144**, 134-140 (1997).
16. Y. Lee, J. Kim, Y. Lee, I. Kim, H. Moon, J. Park, C. P. Jacobson, and S. J. Visco, *Journal of Power Sources*, **115**, 219-228 (2003).
17. X. J. Chen, S. H. Chan, and K. A. Khor, *Solid State Ionics*, **164**, 17-25 (2003).
18. A. Mitterdorfer and L. J. Gauckler, *Solid State Ionics*, **111**, 185-218 (1998).
19. T. Horita, K. Yamaji, H. Negishi, N. Sakai, H. Yokokawa, and T. Kato, *Solid State Ionics*, **137**, 897-904 (2000).
20. M. Kuznecov, P. Otschik, P. Obenaus et al., *Solid State Ionics*, **157**, 371-378 (2003).
21. S. M^{c}Intosh, S. B. Adler, J. M. Vohs, and R. J. Gorte, *Electrochem & Sol-State Letters*, **7** (2004) A111-A114.
22. S. P. Jiang and W. Wang, *Electrochem & Sol-State Letters*, **8**, A115 (2005).
23. K. Yasumoto, N. Mori, J.Mizusaki, H. Tagawa, M. Dokiya, *J. Electrochemical Soc.*, **148**, A105 (2001).
24. X. J. Chen, S. H. Chan, K. A. Khor, *Electrochem & Sol-State Letters*, **7**, A147 (2006).

25. M. Sase, D. Ueno, K. Yashiro, A. Kaimai, T. Kawada, J. Mizusaki, *J. Phys. Chem. Sol.*, **66**, 343 (2005).
26. Y. Huang, J. M. Vohs, and R. J. Gorte, *Electrochem & Sol-State Letters*, **9**, A237 (2006).
27. M. Mogensen and P. V. Hendriksen, *Electrochemical Society Proceedings*, Volume 2003-07, pp 1126.
28. R. J. Kee, H. Zhu, and D. G. Goodwin, *Proceedings of the Combustion Institute*, **30**, 2379 (2005).

Figure Captions:

1a) V-i curves measured at 973 K, with 15% H_2O in H_2 at the Co-ceria-YSZ counter electrode and a $P(O_2)$ = 1 atm at the perovskite-based electrode. Data are for YSZ composites with LSM (□), LSF (○), and LSCo (Δ).

1b) Impedance measurements at 140 mA/cm^2 (electrolysis), with 15% H_2O in H_2 at the Co-ceria-YSZ counter electrode and a $P(O_2)$ = 1 atm. The anodes were composites of YSZ with the following: LSM (□), LSF (○), and LSCo (Δ).

2) V-i curves as a function of polarization history with an LSM-YSZ anode (pasted), with 15% H_2O in H_2 at the Co-ceria-YSZ counter electrode and a $P(O_2)$ = 0.21 atm: □--before polarization; ○--immediately after fuel-cell polarization at 570 mA/cm^2 for 1h; Δ--after electrolysis at 285 mA/cm^2 for 24h.

3) Impedance spectra as a function of polarization history with an LSM-YSZ anode (pasted), with 15% H_2O in H_2 at the Co-ceria-YSZ counter electrode and a $P(O_2)$ = 0.21 atm: ■--before polarization; □--immediately after fuel-cell polarization at 570 mA/cm^2 for 1h; after electrolysis-mode at 285 mA/cm^2 for ●--10 min, ○--30 min, Δ--60 min, ▲--120 min, and ◊--180 min.

4) Cell potential and electrode impedance as a function of time, for an electrolysis current density of 285 mA/cm^2, using an LSM-YSZ anode (pasted), with 15% H_2O in H_2 at the Co-ceria-YSZ counter electrode and a $P(O_2)$ = 0.21 atm: ■--potential; ○--electrode impedance.

5) Cell potential as a function of time, for an electrolysis current density of 285 mA/cm^2, using an LSF-YSZ anode, with 15% H_2O in H_2 at the Co-ceria-YSZ counter electrode and a $P(O_2)$ = 0.21 atm.

6a) Impedance spectra at 973 K for an LSF-YSZ electrode operating at a $P(O_2)$ = 1 atm and a Co-ceria-YSZ electrode in 15%H_2O + H_2. The dc current densities were: 30 (□), -30 (○), –145 (Δ), -430 mA/cm^2 (◊), with negative currents signifying electrolysis mode of operation.

6b) Impedance spectra at 973 K for an LSCo-YSZ electrode operating at a $P(O_2)$ = 1 atm and a Co-ceria-YSZ electrode in 15%H_2O + H_2. The dc current densities were: 30 (□), -30 (○), and –145 (Δ), with negative currents signifying electrolysis mode of operation.

7a) V-i curves measured at 973 K with 15% H_2O in H_2 at the Co-ceria-YSZ counter electrode and N_2 (○) or O_2 (Δ) at LSF-YSZ electrode.

7b) V-i curves measured at 973 K with 15% H_2O in H_2 at the Co-ceria-YSZ counter electrode and N_2 (○) or O_2 (□) at LSCo-YSZ electrode.

Figure1a

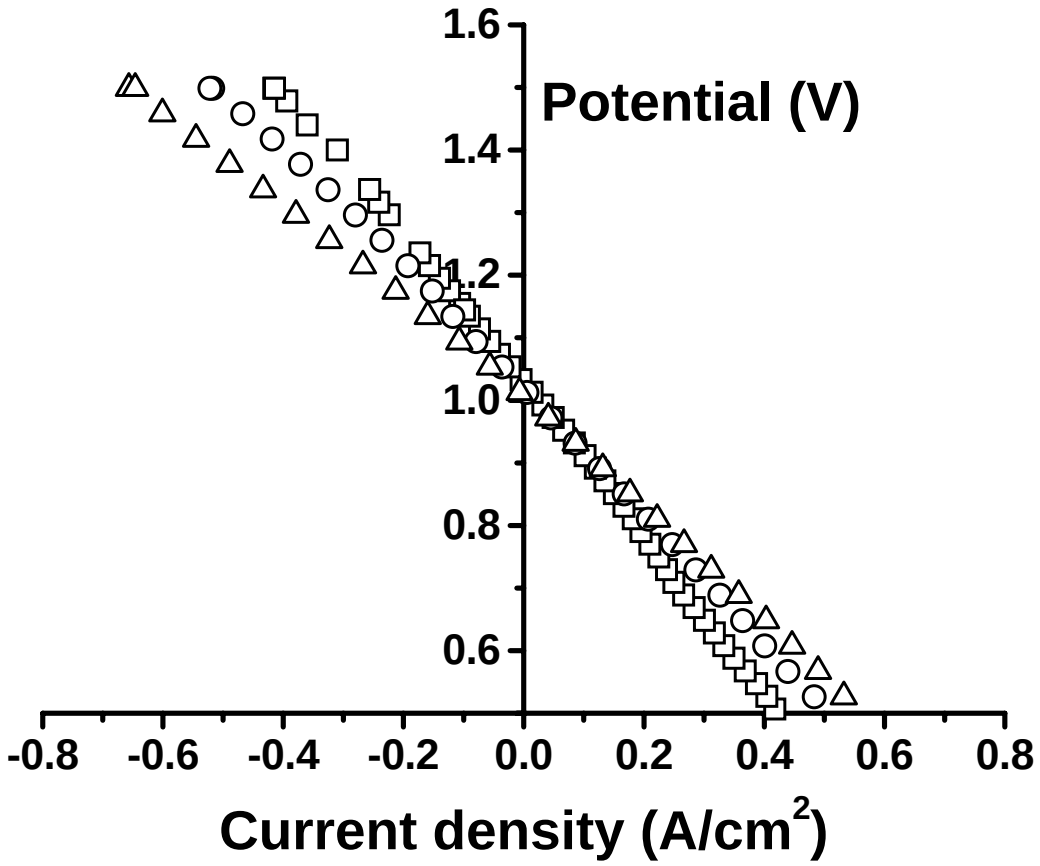
1.6
1.4
1.2
1.0
0.8
0.6
Potential (V)
-0.8
-0.6
-0.4
-0.2
0.0
0.2
0.4
0.6
0.8
Current density (A/cm2)

Figure 1b

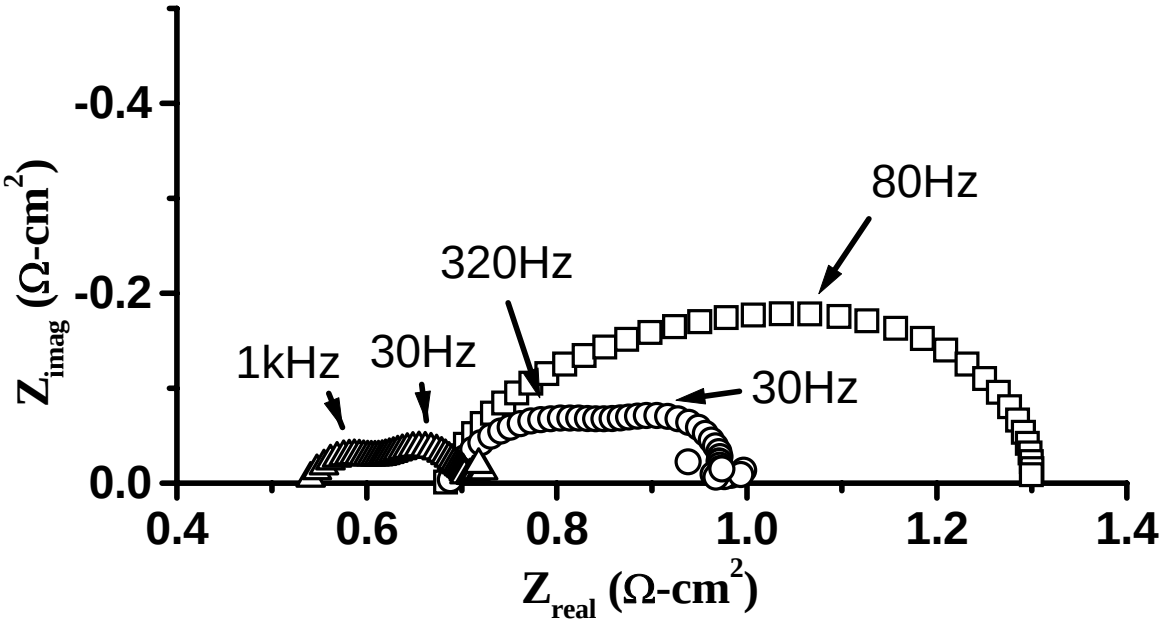
-0.4
-0.2
0.0
0.4
0.6
0.8
1.0
1.2
1.4
Z_{imag} (Ω-cm^2)
Z_{real} (Ω-cm^2)
80Hz
320Hz
1kHz
30Hz
30Hz

Figure 2

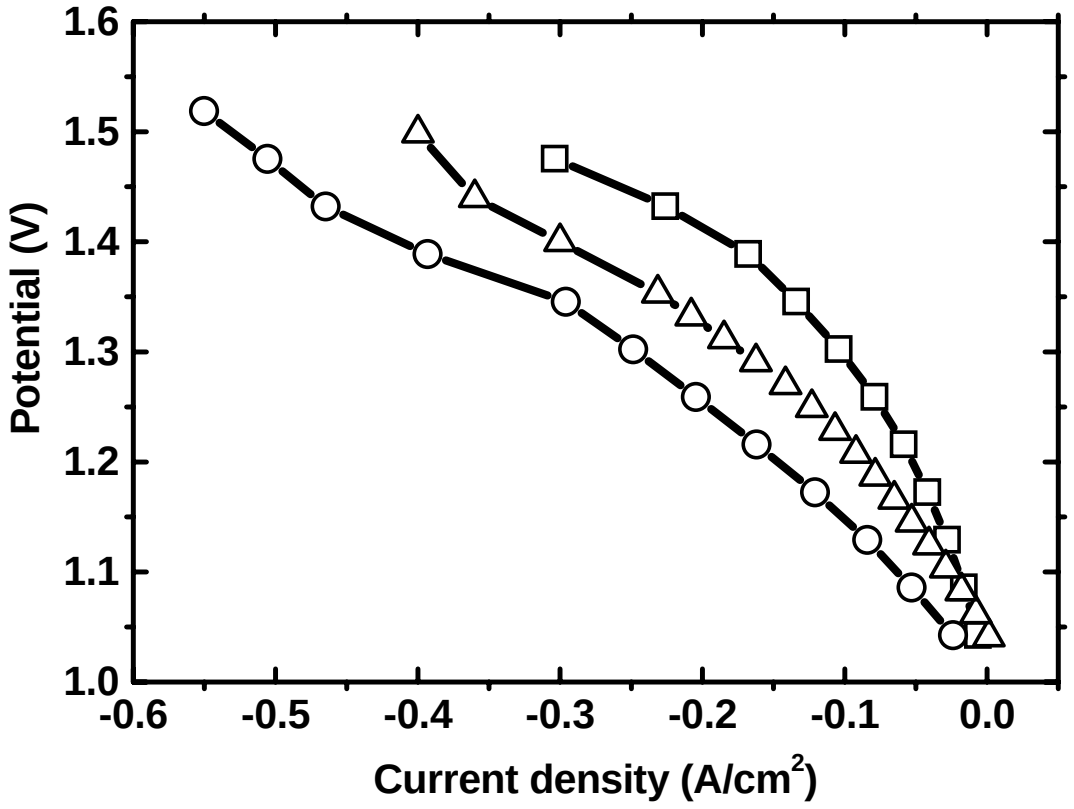
1.6
1.5
1.4
1.3
1.2
1.1
1.0
Potential (V)
-0.6
-0.5
-0.4
-0.3
-0.2
-0.1
0.0
Current density (A/cm2)

Figure 3

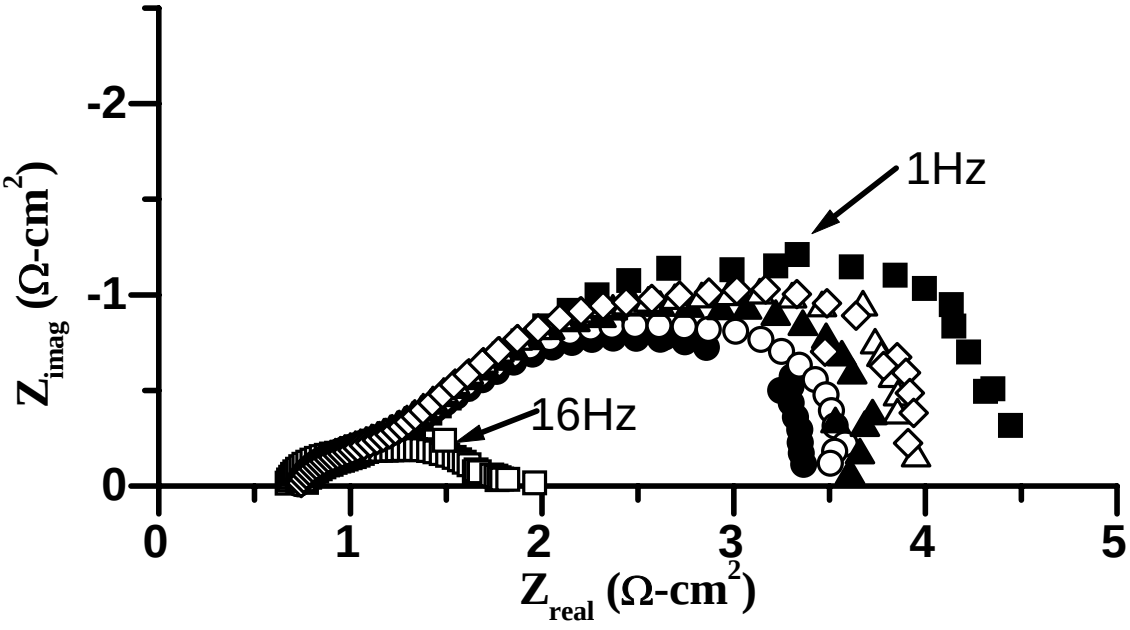

Figure 4

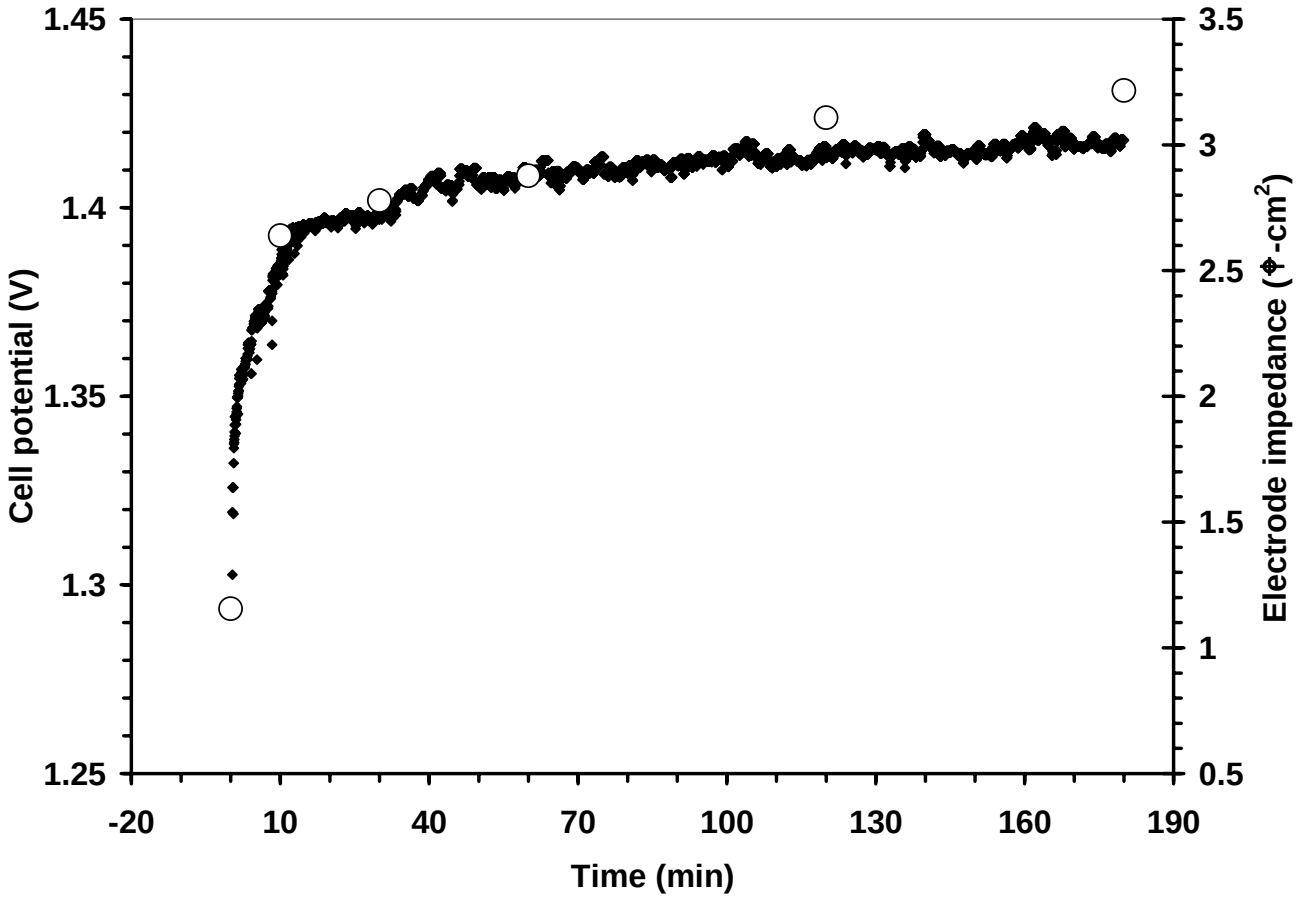
1.45
1.4
1.35
1.3
1.25
Cell potential (V)
3.5
3
2.5
2
1.5
1
0.5
Electrode impedance (Ω-cm²)
-20
10
40
70
100
130
160
190
Time (min)

Figure 5

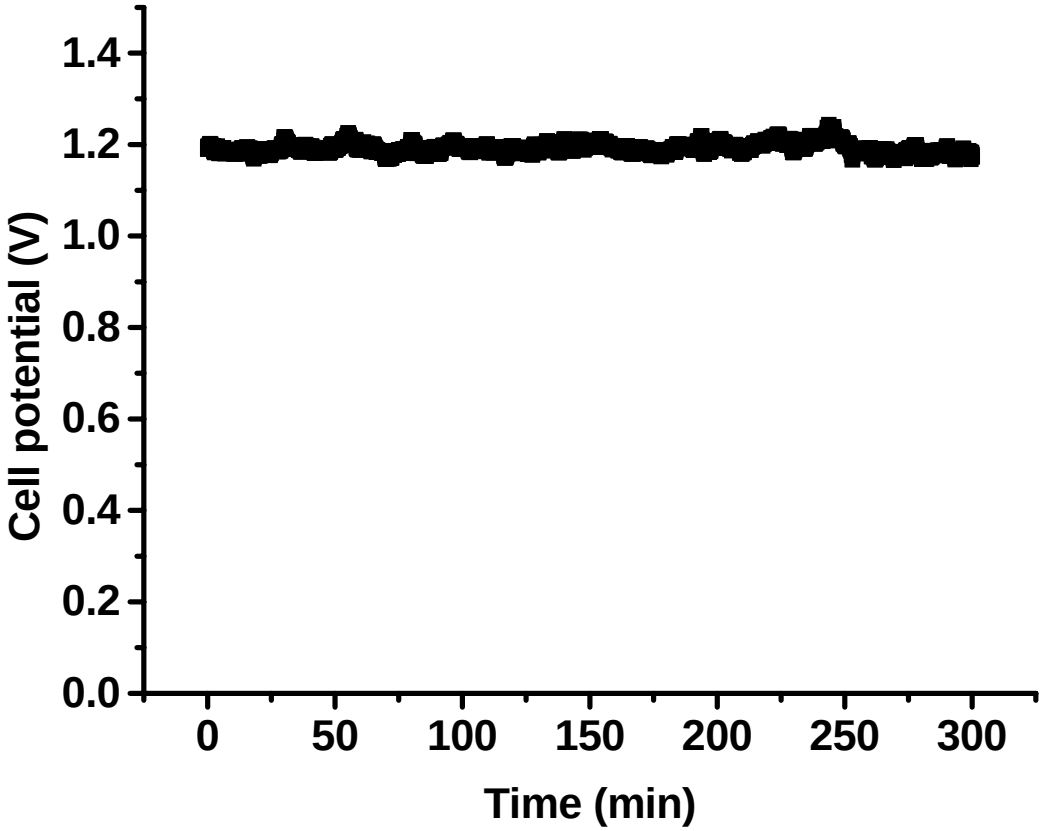
Cell potential (V)
1.4
1.2
1.0
0.8
0.6
0.4
0.2
0.0
0
50
100
150
200
250
300
Time (min)

Figure 6a

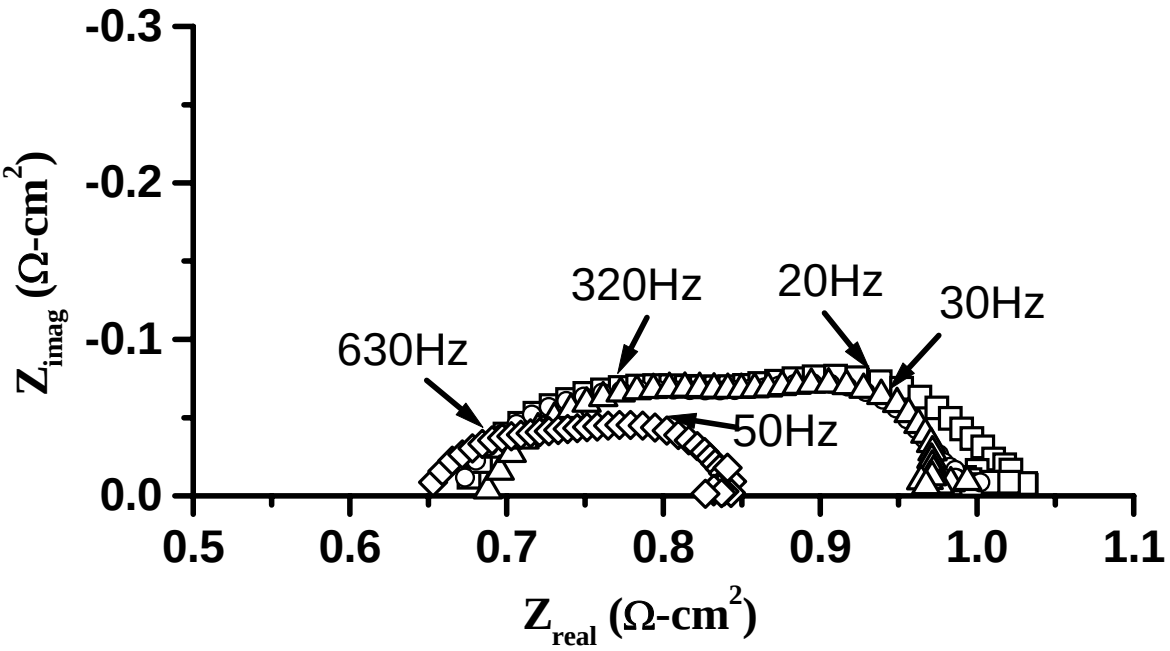
-0.3
-0.2
-0.1
0.0
0.5
0.6
0.7
0.8
0.9
1.0
1.1
Z_{imag} (Ω-cm^2)
Z_{real} (Ω-cm^2)
630Hz
320Hz
20Hz
30Hz
50Hz

Figure 6b

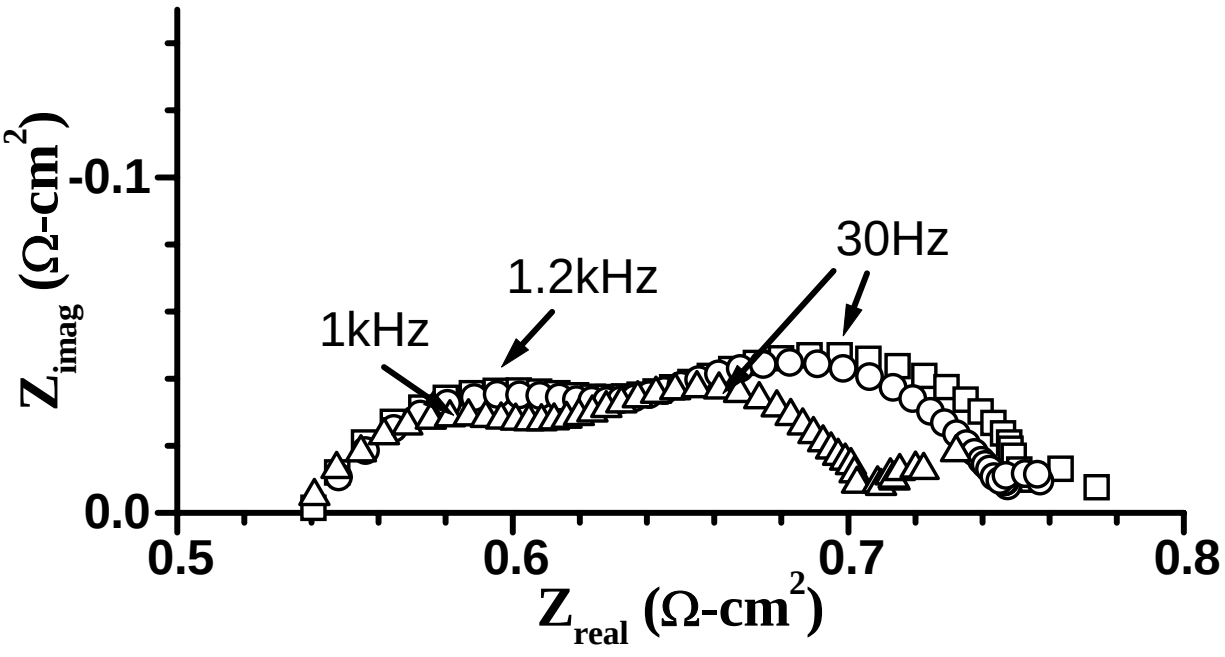
-0.1
0.0
0.5
0.6
0.7
0.8
Z_{imag} (Ω-cm^2)
Z_{real} (Ω-cm^2)
1kHz
1.2kHz
30Hz

Figure 7a

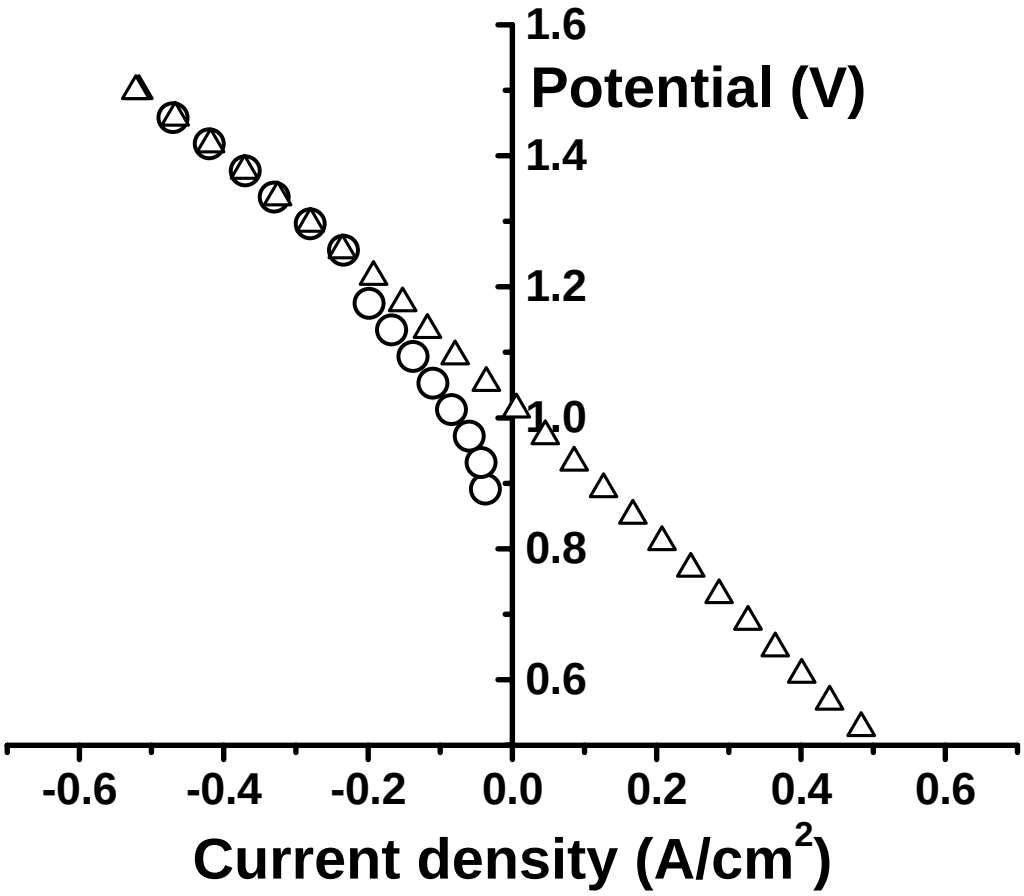
1.6
Potential (V)
1.4
1.2
1.0
0.8
0.6
-0.6
-0.4
-0.2
0.0
0.2
0.4
0.6
Current density (A/cm2)

Figure 7b

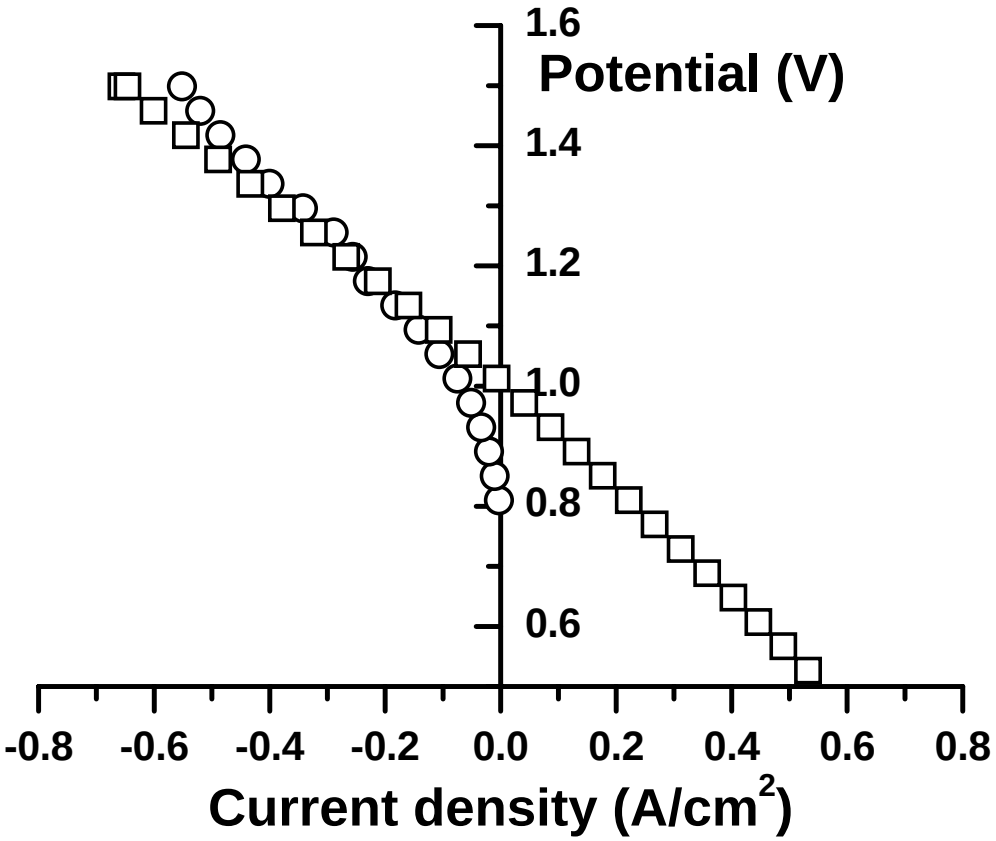
1.6
Potential (V)
1.4
1.2
1.0
0.8
0.6
-0.8
-0.6
-0.4
-0.2
0.0
0.2
0.4
0.6
0.8
Current density (A/cm2)